A Flush-Mounted Dual-Axis Wall Shear Stress Sensor

Brett R. Freidkes, David A. Mills, William C. Patterson, Philip M. Fournier, and Mark Sheplak, *Member, IEEE*

***Abstract*— This paper presents the fabrication, packaging, and calibration of a flush-mounted, dual-axis, differential capacitive wall shear stress sensor. The two-mask fabrication process produces a 7-mm die with a 2-mm by 2-mm floating element supported by eight, compliant crab-leg tethers. Taking advantage of backside wire bonds, the hydraulically smooth package is suitable for wind tunnel testing and is designed to have a resonant frequency of 3.7 kHz. Initial dynamic calibration data are presented using both single-ended and fully-differential electronics, with sensitivities as high as 80 mV/Pa and minimum detectable wall shear stress values as low as 10 μPa/Hz$^{1/2}$, resulting in dynamic ranges near 135 dB. [2020-0175]**

***Index Terms*— Acoustic plane wave tube, backside wire bonds, capacitive transduction, crab-leg tethers, fully-differential biasing, single-ended biasing, wall shear stress.**

I. INTRODUCTION

THE measurement of wall shear stress is a critical component of understanding complex flow phenomena, including flow separation, viscous drag, and boundary layer physics. Indirect sensors, including those determining wall shear stress based on heat flux or pressure gradients, have provided experimental information on wall shear stress but require empirical relationships and assumptions that may be invalid, particularly in unknown, three-dimensional flow environments [1], [2]. Direct sensors, such as the one presented in this manuscript, are a solution to making continuous vector measurements of wall shear stress by providing voltage outputs that are calibrated against a known wall shear stress.

Significant progress has been made in the field of one-dimensional, direct wall shear stress sensors, including those of a differential, capacitive nature [3], [4]. These improvements in shear stress sensing technology have provided insight into turbulent boundary layers and may have implications in flow control applications [5], [6]. In general, these transducers are restricted to one measurement axis, and the development of a dual-axis sensor has been limited. In 2003, Tseng and Lin [7] developed a two-axis optical device that takes advantage of Fabry-Perot interferometry. The waterproof sensor showed a minimum detectable signal of 65 mPa for a spectrometer resolution of 0.1 nm. Despite its ability to measure two-dimensional wall shear stress signals in both water and air, its sensitivity to temperature and vibrations may prove problematic during wind tunnel testing. Later, Adcock *et al.* [8] fabricated a two-axis gimbal structure that incorporated piezoresistors into torsional hinges. Preliminary results demonstrated minimal temperature sensitivity but did not include AC calibration data. Barnard *et al.* [9] continued research in the field by producing the first-ever dual-axis capacitive shear stress sensor; however, this device was produced as a proof-of-concept and was not suitable for wind-tunnel testing, as it featured frontside wire bonds and a printed-circuit-board (PCB) package. These frontside wire bonds intruded into the flow field, potentially violating the assumption of hydraulic smoothness, and the PCB package was large and allowed for excess drift and noise in the output signal. Additionally, the sensor structure was asymmetric, leading to an increase of parasitic capacitance and a decrease in sensor sensitivity.

Freidkes *et al.* [10] improved the sensor by Barnard *et al.* by redesigning the sensor die to be symmetric, incorporating backside wire bonds to produce a flusher surface, and utilizing a package similar to the one-dimensional device created by Mills *et al.* [4], [11]. The resulting device, however, was slightly tilted in the package, causing a 50-μm step that favored the sensitivity of one sensing direction over the other. More recently, Mills *et al.* [12] improved on this package and discussed the advantages and disadvantages of various circuit topologies. This paper focuses on the fabrication, packaging, and calibration results for a similar device with crab-leg tethers and compares the results of both single-ended and fully-differential interface circuit schemes.

II. SENSOR STRUCTURE

An illustration of the sensor is shown in Fig. 1. A floating element, supported by eight identical crab-leg tethers, deflects in response to an incident wall shear stress. Interdigitated

Manuscript received May 15, 2020; revised July 5, 2020; accepted July 6, 2020. Date of publication July 20, 2020; date of current version October 7, 2020. This work was supported in part by the NSF I/UCRC on Multi-functional Integrated System Technology (MIST) Center under Grant IIP-1439644, Grant IIP-1439680, and Grant IIP-1738752, in part by the NASA SBIR under Grant 80NSSC18P1901, and in part by the National Science Foundation Graduate Research Fellowship under Grant DGE-1315138 and Grant DGE-1842473. Subject Editor M. Rais-Zadeh. *(Corresponding author: Brett R. Freidkes.)*

Brett R. Freidkes is with the Mechanical and Aerospace Engineering Department, University of Florida, Gainesville, FL 32611 USA (e-mail: bfreidkes@ufl.edu).

David A. Mills, William C. Patterson, and Philip M. Fournier are with the Interdisciplinary Consulting Corporation, Gainesville, FL 32609 USA (e-mail: dmills@thinkic2.com; cpatterson@thinkic2.com).

Mark Sheplak is with the Mechanical and Aerospace Engineering Department, University of Florida, Gainesville, FL 32611 USA, and also with the Electrical and Computer Engineering Department, University of Florida, Gainesville, FL 32611 USA (e-mail: sheplak@ufl.edu).

Color versions of one or more of the figures in this article are available online at http://ieeexplore.ieee.org.

Digital Object Identifier 10.1109/JMEMS.2020.3008471

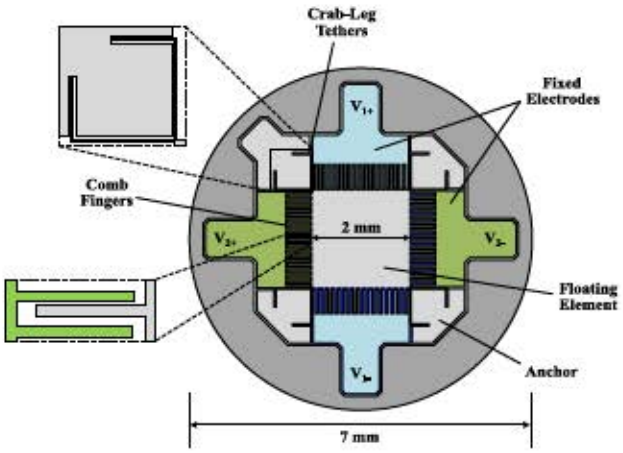

Fig. 1. Illustration of the sensor structure, with emphasis on the biasing of the fixed electrodes, the crab-leg tethers, and the variable-gap capacitors.

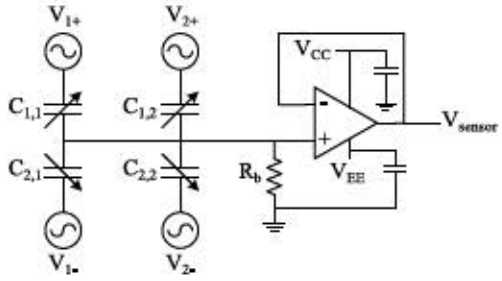

Fig. 2. Single-ended circuit schematic with a voltage amplifier. The four static electrodes are each biased and the output is taken from the floating element.

comb fingers between the floating element and four fixed electrodes form variable-gap capacitors that change depending on the direction of the wall shear stress vector. The sensor is designed to be differential, i.e., when the floating element deflects, the gaps on one side of the element will shrink while the gaps on the opposing side grow. Such a design improves common-mode rejection, e.g., normal pressure, and overall device sensitivity.

The interface circuitry associated with this sensor die is grouped into two categories: single-ended versus fully-differential. For the single-ended case, shown in Fig. 2 with a voltage amplifier, high-frequency sine waves bias the four fixed electrodes and the output is tied to the floating element. For one axis, a 900 kHz sine wave and its 180° complement bias the electrodes (respectively depicted as V_{1+} and V_{1-}) while the second axis features the same biasing but at a frequency of 1 MHz. A bias resistor is present to establish a DC operating point and to prevent amplifier saturation.

The fully-differential case, shown in Fig. 3, biases the floating element at a single frequency while providing outputs from the four fixed electrodes. These two pairs of outputs are ultimately fed into fully-differential amplifiers to remove common-mode signals, such as normal pressure or power line noise. Due to the high output impedance of the sensor, the voltage output for both cases requires buffering close to the sensor head to minimize signal degradation associated

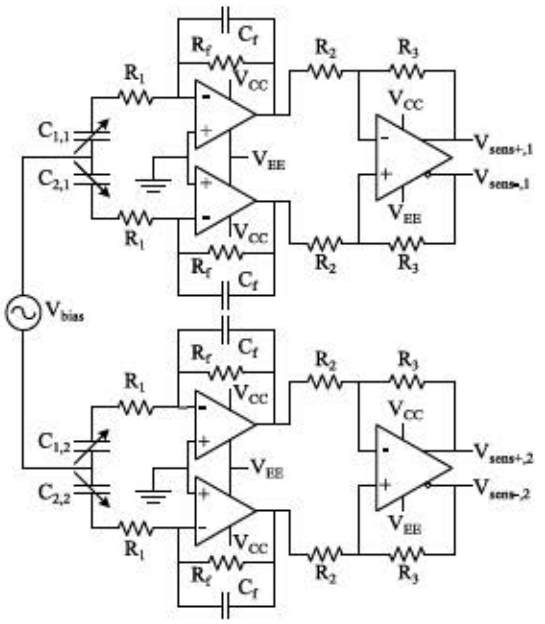

Fig. 3. Fully-differential circuit schematic with charge amplifiers. The floating element is biased, and each static electrode creates an output that is buffered in a charge amplifier and then tied to a fully-differential amplifier.

with transmission. This is accomplished by using either a voltage amplifier (shown in Fig. 2) or several charge amplifiers (shown in Fig. 3). More detail on these biasing schemes and the synchronous modulation/demodulation (SMOD/DMOD) process used to measure both AC and DC wall shear stress is presented by Mills *et al.* [12] and is omitted here.

The device discussed in this paper features crab-leg tethers, as shown in the top left corner of Fig. 1. Previous work [10], [12] utilized serpentine tethers due to their success in accelerometers [13] and the ability to easily alter resonance targets by changing the number of meanders. Additionally, the serpentine tethers may achieve the same stiffness in a smaller footprint compared to crab-leg flexures. Despite the benefits of serpentine tethers, preliminary simulation results indicate that sensors with this flexure geometry are more sensitive to normal pressure than ones with crab-leg tethers. This is very important for measuring wall shear stress considering that normal pressure may produce extraneous outputs or cause the floating element to no longer be flush with the boundary.

Mechanical coupling between axes is minimized with the new tether structure by designing the die to be symmetric with eight tethers. Despite this, coupling between the axes will still exist due to fabrication tolerances and electrostatic coupling. The latter occurs due to the behavior of the interdigitated capacitors, i.e., when the floating element displaces in one direction, the capacitive gaps on two sides of the element will change while the capacitive overlap area will change for the other sides. To minimize the electrostatic coupling, the nominal overlap length is designed to be much larger than the nominal gap distance, as the percent change in capacitance will be much less for the secondary axis compared to the main axis.

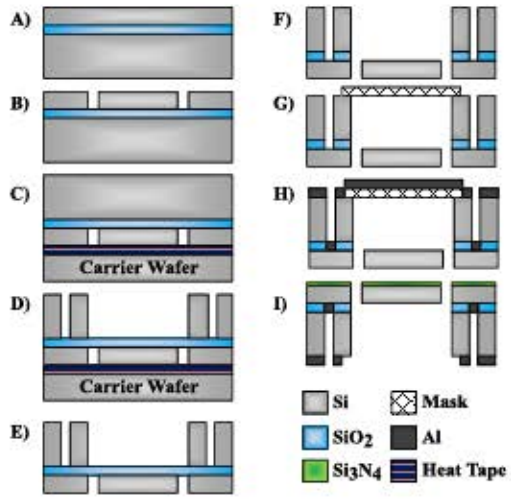

Fig. 4. Process traveler of the 2D sensor with backside contacts.

In order to quantify the coupling between axes, a cross-axis rejection ratio,

$$S_{2,1} = 20\log_{10}\left(\frac{S_1}{S_2}\right) \tag{1}$$

is defined. In (1), S_1 is the sensitivity of the on-axis direction, i.e., the direction aligned with the flow, while S_2 is the sensitivity of the off-axis direction during the same testing run. The notation $S_{2,1}$ signifies the response of the second axis when the first axis is aligned with the flow.

Additionally, a pressure rejection ratio, $H_{P,1}$, defined by

$$H_{P,1} = 20\log_{10}\left(\frac{S_1}{S_{P,1}}\right), \tag{2}$$

quantifies the response of an axis to normal pressure. In (2), $S_{P,1}$ is the sensitivity of the first axis to pressure and S_1 is the sensitivity of the same axis to wall shear stress. A pressure rejection ratio is also found for the second axis.

Both the cross-axis rejection ratios and the pressure rejection ratios are used to compare the results of the previous work with serpentine tethers to the current work featuring crab-leg tethers. The ratios are also used to demonstrate the differences in circuit topologies.

III. Fabrication

The first dual-axis sensor fabricated by Barnard *et al.* [9] had frontside wire bonds, limiting its use in certain flow conditions due to disturbances caused by their protrusion into the flow. Additionally, three photolithography steps were required, making fabrication more time consuming and prone to additional failures. The fabrication process presented here, shown in Fig. 4, requires only two photolithography steps due to its incorporation of backside wire bonds.

A silicon-on-insulator (SOI) wafer with a device layer of 60 μm (boron-doped to a resistivity less than 0.005 Ω-cm), a buried-oxide layer (BOX) of 2 μm, and a handle layer of 500 μm (boron-doped to a resistivity of 30 Ω-cm) is chosen and is depicted Fig. 4A. The first photolithography step, shown in Fig. 4B, allows for a deep-reactive ion etch (DRIE) of the frontside features (the floating element, tethers, comb fingers, etc.) into the device layer. A fast etch recipe is initially used for the majority of the DRIE, followed by a second recipe that minimizes footing near the BOX layer which impacts tether compliance and sensor performance. Additionally, this frontside mask is designed to create circular die that separate after all etching steps, eliminating the need for a dicing saw.

The wafer is flipped over and attached to a carrier wafer via Nitto-Denko 3195H 150°C thermal release tape, as shown in Fig. 4C. This carrier wafer is required to protect the frontside of the wafer during future steps and to provide structural support once the device layer and handle layer are etched. Care is taken during the application of the tape in order to minimize air bubbles caught between the wafers, as these air bubbles may cause thermal stresses that break the wafer during the following etch.

The handle layer is etched in the DRIE in Fig. 4D, where the patterning includes the backside of the floating element (ultimately allowing for movement of the structure) and six backside holes for wire bonding access to the four fixed electrodes, the floating element, and the ground plane. To separate the die, the heat tape is activated by placing the carrier wafer on a 150°C plate for ten seconds. During this process, the 2-micrometer BOX layer is broken, and the die are separated by design.

Next, the exposed BOX layer must be removed to release the floating element. This is performed via a 49% hydrofluoric (HF) acid vapor etch, where the devices are elevated above the acid for 10 minutes. To remove any remnant HF afterwards, a triple rinse in isopropyl alcohol is performed prior to a carbon dioxide critical point dry.

After the BOX etch in Fig. 4F, metal must be sputtered into the backside holes for wire bonding during the packaging process. An aluminum shadow mask is used to cover and protect the exposed floating element, as shown in Fig. 5. Within a Kurt Lesker sputterer, 500 nm of aluminum is deposited into the six backside holes.

After backside metal deposition, a 100 nm silicon nitride layer is deposited on the front of the devices via plasma-enhanced chemical vapor deposition (PECVD). This coating serves as a moisture barrier and helps reduce sensitivity to changes in humidity. Lastly, to ensure ohmic contact between the sputtered metal and the backside of the device layer, a contact anneal is performed in forming gas (5% H_2 in N_2) for 30 seconds at 460°C using a rapid thermal annealing system.

IV. Packaging

The packaging of the device, shown in Fig. 6, is novel in that it incorporates backside wire bonds as opposed to through-silicon-vias, which may be costly. The die is epoxied to a PCB and wire bonded through the handle layer to the sputtered metal on the backside of the device layer. An Omnetics Polarized Nano connector is soldered to the board and interfaces with a wire harness that feeds into a stainless-steel cylindrical housing.

The interior of the housing contains another PCB that features voltage amplifiers (used in the single-ended topology)

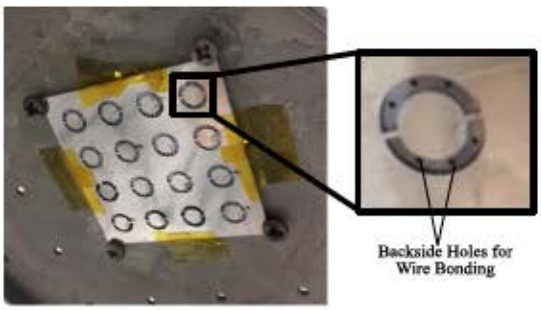

Fig. 5. Aluminum shadow mask used during sputter deposition.

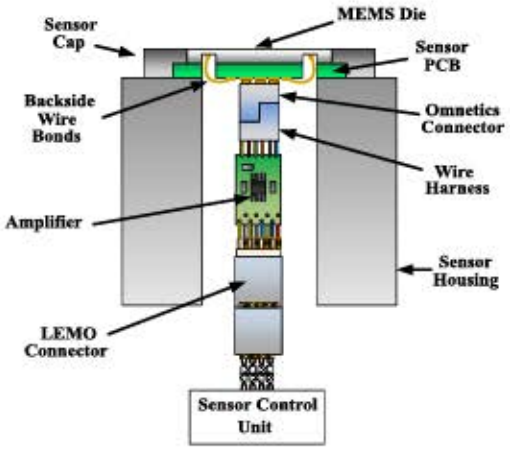

Fig. 6. Full packaging schematic of the dual-axis wall shear stress sensor with backside wire bonds.

or charge amplifiers (used in the fully-differential topology). Locating this PCB close to the sensor head minimizes signal degradation associated with the transmission of a high-frequency, high-impedance signal. Also present on this PCB are filtering capacitors used to reduce ripples in the operational amplifier power supply lines.

The completed amplifier board is permanently placed inside of the 15.9-mm outer diameter, 11-mm inner diameter, stainless-steel housing using an arbor press. The outer surface of the housing features a 2-mm keyway to ensure proper orientation of the sensor relative to the flow. Additionally, the housing outer diameter reduces to 12.7 mm near the sensing end to provide a mechanical hard stop for a repeatable, flush installation. The multi-pin connector on the back of the housing connects via a multi-conductor shielded cable to a sensor control unit that houses the interfacing circuitry and performs the SMOD/DMOD process [12]. The finished package is shown in Fig. 7.

A scanning white light interferometer (SWLI) is used to examine the roughness of the sensor head. Knowing the flushness of the device determines the range of flow speeds for which the assumption of hydraulic smoothness is valid. The SWLI results in Fig. 8 and Fig. 9 show that the sensor is flush to within 10 micrometers in the x-direction and to within 20 micrometers in the y-direction. A slight tilt does exist along the y-axis; however, these results are a significant

Fig. 7. Completed sensor package.

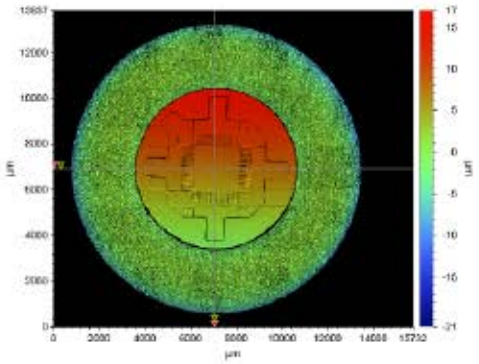

Fig. 8. SWLI image of the sensor head.

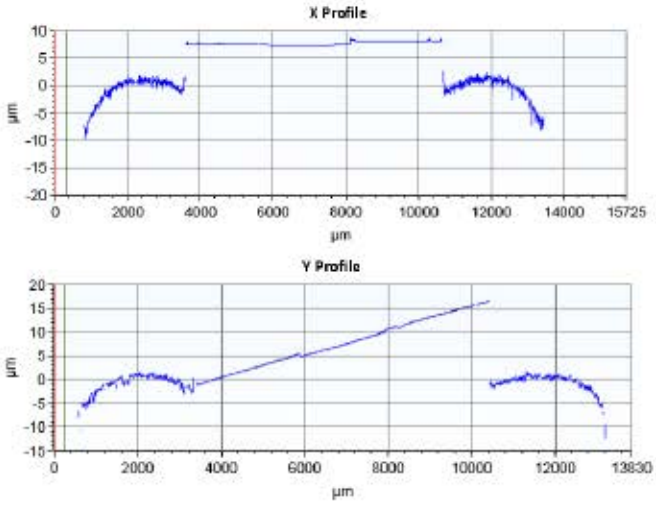

Fig. 9. Sensor topography profile along the x-axis (top) and y-axis (bottom). The x-axis remains flush to within 10 μm while the y-axis is flush to within 20 μm with a slight tilt.

improvement compared to the work previously presented by Freidkes *et al.* [10].

V. Results

The dynamic calibration of the wall shear stress sensor is performed within an acoustic plane wave tube, where sound waves produce a frequency-dependent boundary layer [14]. To calibrate each axis and to quantify cross-axis sensitivities, the device is rotated in increments of 45° so that the incident wall shear stress vector perturbs the floating element in

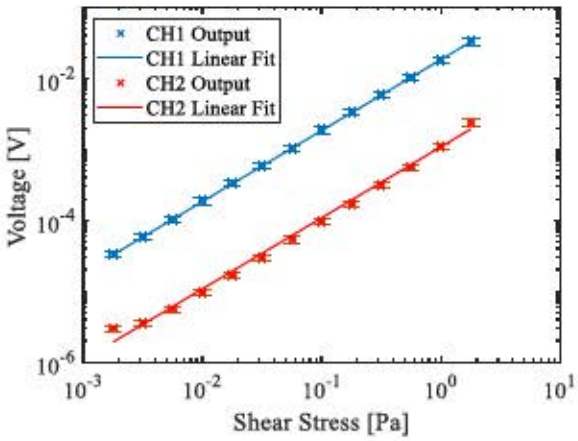

Fig. 10. Sensitivity curve for the single-ended circuit topology at a sensor orientation of 0°.

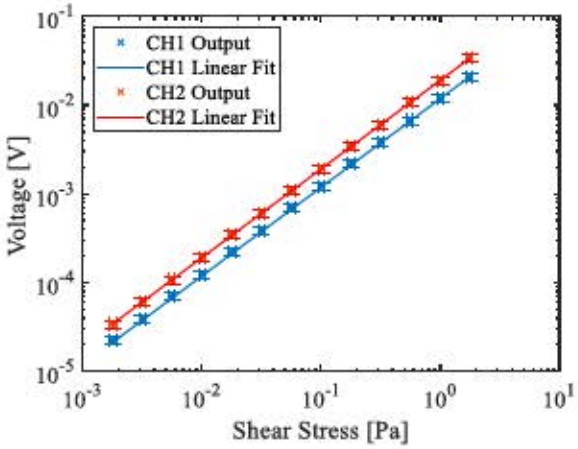

Fig. 11. Sensitivity curve for the single-ended circuit topology at a sensor orientation of 45°.

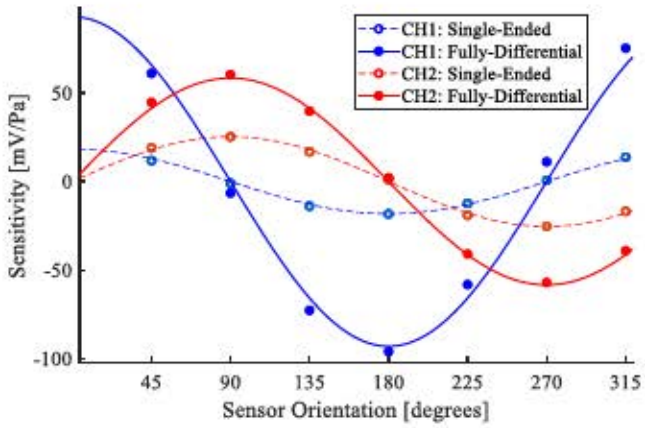

Fig. 12. Wall shear stress sensitivities for the different circuitries as a function of sensor orientation. Fitted sinusoids are shown for illustrative purposes.

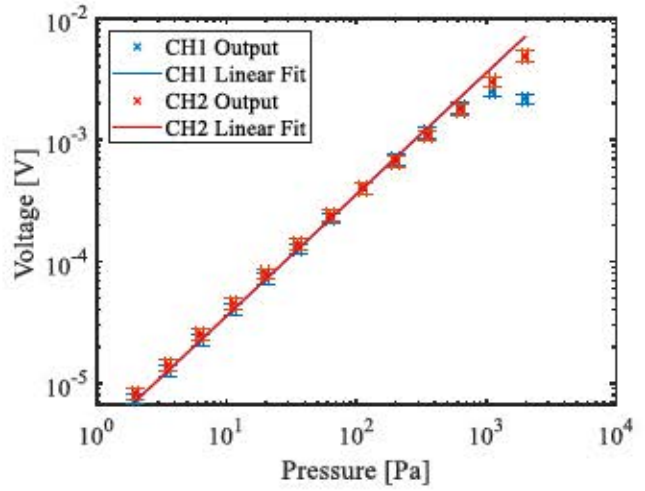

Fig. 13. Pressure sensitivity curve for the single-ended circuit topology.

different directions, causing associated capacitance changes. Sensitivity curves are produced by increasing the sound pressure level within the plane wave tube, as larger sound pressure levels increase the wall shear stress acting on the sensor head.

Fig. 10 shows the calibration results at 1 kHz of the single-ended voltage-amplifier topology for the 0° orientation, where one axis is aligned with the flow (CH1) and is the main sensing direction and the second axis (CH2) is perpendicular to the flow and would ideally show zero output.

Fig. 11 shows the same calibration but for the case where the sensor is oriented at a 45° angle. For these diagonal calibrations, the response of the sensor should ideally be the same for each axis, with a 180° phase difference between the axes for the 135°/225° tests. This 180° phase offset is represented by a negative sign in the sensitivity.

The calibration is repeated in increments of 45° for both the single-ended and fully-differential interface circuitries at a test frequency of 1 kHz. The results of both calibrations as a function of sensor orientation are shown in Fig. 12.

To determine the sensitivity of the device to normal pressure, the calibration is performed in a manner similar to that of the shear stress testing, i.e., the sensor is placed in an acoustic plane wave tube and the pressure is increased to produce sensitivity curves. For this test, however, the sensor is placed in the rigid end wall of the plane wave tube where it is subjected to normal pressure sans tangential stresses [12]. Fig. 13 shows the calibration results using the single-ended circuitry at an acoustic frequency of 1 kHz.

Finally, the noise floor of each axis was recorded in a quiescent plane wave tube at a sampling frequency of 50 kHz with 1 Hz bins. Utilizing the average dynamic sensitivity at 1 kHz for each sensing axis, the noise floors are used to determine the minimum detectable signal (MDS) versus frequency. Shown in Fig. 14 for the single-ended and the fully-differential schemes, all MDS versus frequency curves show considerable flicker ($1/f$) noise.

The calibration results of the serpentine-based sensor from Mills *et al.* [12] are displayed in Table I while the results corresponding to the crab-leg tethered device presented in this work are shown in Table II. First, the sensitivities for the current work are greater due to a larger floating element (larger nominal capacitance) and a smaller primary capacitive gap (3 μm for this work compared to 3.5 μm for the prior work). In response, the MDS for each configuration is lower compared to the previous work.

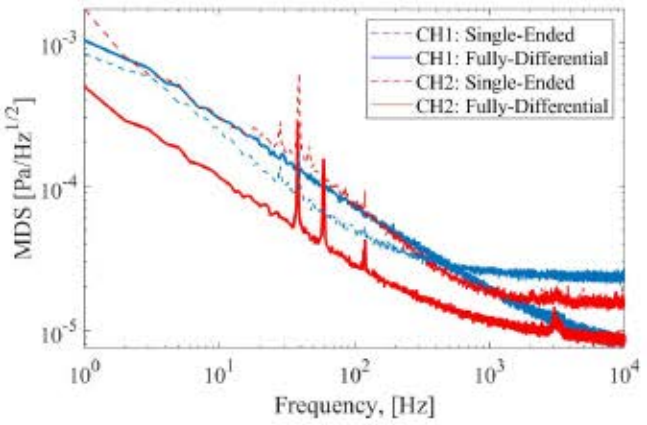

Fig. 14. MDS versus frequency of both axes for the two circuit topologies.

TABLE I
PREVIOUS CALIBRATION RESULTS [12]

	Single-Ended		Fully-Differential	
Sensing Direction	CH1	CH2	CH1	CH2
Shear stress sensitivity, S (mV/Pa)	7.15	7.55	4.24	6.87
Cross-axis sensitivity, S_c (mV/Pa)	0.91	0.56	0.27	0.18
Cross-axis rejection ratio, $S_{x,y}$ (dB)	18.4	22.1	28.3	27.4
Pressure sensitivity, S_P (μV/Pa)	0.57	1.19	0.39	0.96
Pressure rejection ratio, $S_{x,P}$ (dB)	82.0	76.0	80.7	77.1
Noise floor, (μV/Hz$^{1/2}$)	0.37	1.36	0.70	0.40
Minimum detectable signal, (mPa/Hz$^{1/2}$)	0.05	0.18	0.16	0.06

TABLE II
CURRENT CALIBRATION RESULTS

	Single-Ended		Fully-Differential	
Sensing Direction	CH1	CH2	CH1	CH2
Shear stress sensitivity, S (mV/Pa)	18.1	25.3	80.0	58.7
Cross-axis sensitivity, S_c (mV/Pa)	1.12	0.86	8.82	2.53
Cross-axis rejection ratio, $S_{x,y}$ (dB)	27.1	26.5	16.7	30.0
Pressure sensitivity, S_P (μV/Pa)	3.55	3.58	4.22	6.86
Pressure rejection ratio, $S_{x,P}$ (dB)	74.2	77.0	85.6	78.6
Noise floor, (μV/Hz$^{1/2}$)	0.46	0.47	1.83	0.71
Minimum detectable signal, (mPa/Hz$^{1/2}$)	0.03	0.02	0.02	0.01

Ideally, the sensitivities for each axis match but as shown in Table II, there are differences in the results. For the single-ended topology, the voltage biases applied to the static electrodes may not be perfectly balanced, i.e., their amplitudes may be different and therefore, the sensitivities will vary. For the fully-differential circuitry, the multiple charge amplifiers may present slight phase offsets in the signals, which will alter the outputs of the fully-differential amplifiers. Additionally, the tilt shown in Fig. 9 may also be a factor [10].

The pressure rejection ratios have improved for the crab-leg devices, as predicted, for the fully-differential topologies. However, the single-ended circuitry does not show the same trend. Future work will focus on fabricating and testing more crab-leg devices to confirm this behavior or attribute it to process variance.

VI. CONCLUSION

This paper reports the fabrication, packaging, and calibration results for a MEMS-based, capacitive, dual-axis wall shear stress sensor. The fabrication process requires only two photolithography steps and produces a 7-mm circular die that is compatible in a flush-mount package. This novel package takes advantage of backside wire bonds in order to remain smooth to within 20 μm.

The work presented demonstrates significant progress in the field of dual-axis wall shear stress sensing. The research and development of this technology will enable the measurement of complex, three-dimensional wall-bounded turbulent flows and will contribute to the elucidation of the fundamental mechanisms governing unsteady skin friction [6].

Future work looks to continue improving the circuitry associated with each topology. Specifically, the fully-differential configuration has yielded higher sensitivities and lower MDS compared to the single-ended topology, so care will be taken to improve the balancing of this scheme and the circuit components present within it. Environmental testing will be performed to determine temperature and humidity sensitivities as well. Lastly, the target resonance of 3.7 kHz for this sensor will be experimentally verified in a wind tunnel environment.

REFERENCES

[1] J. H. Haritonidis, "The measurement of wall shear stress," in *Advances in Fluid Mechanics Measurements*. Springer-Verlag, 1989, pp. 229–261.
[2] J. W. Naughton and M. Sheplak, "Modern developments in shear-stress measurement," *Prog. Aerosp. Sci.*, vol. 38, nos. 6–7, pp. 515–570, Aug. 2002.
[3] V. Chandrasekharan, J. Sells, J. Meloy, D. P. Arnold, and M. Sheplak, "A microscale differential capacitive direct wall-shear-stress sensor," *J. Microelectromech. Syst.*, vol. 20, no. 3, pp. 622–635, Jun. 2011.
[4] D. Mills, C. Barnard, and M. Sheplak, "Characterization of a hydraulically smooth wall shear stress sensor for low-speed wind tunnel applications," in *Proc. 55th AIAA Aerosp. Sci. Meeting*, Grapevine, TX, USA, 2017, p. 0478.
[5] M. G.-E. Hak, *Flow Control: Passive, Active, and Reactive Flow Management*, 1st ed. Cambridge, MA, USA: Cambridge Univ. Press, 2000, pp. 209–210.
[6] R. J. Pabon, L. Ukeiley, M. Sheplak, and C. B. Keane, "Characteristics of turbulent boundary layer large scale motions using direct fluctuating wall shear stress measurements," *Phys. Rev. Fluids*, vol. 3, no. 11, Nov. 2018, Art. no. 114604.
[7] F.-G. Tseng and C.-J. Lin, "Polymer MEMS-based Fabry–Pérot shear stress sensor," *IEEE Sensors J.*, vol. 3, no. 6, pp. 812–817, Dec. 2003.
[8] E. E. Adcock, M. A. Scott, and S. S. Bajikar, "A two-axis direct fluid shear stress sensor," Nat. Aeronaut. Space Admin., Hampton, VA, USA, Tech. Rep. NASA/TM-2010-216696, May 2010.
[9] C. Barnard, D. Mills, and M. Sheplak, "A system for vector measurement of aerodynamic wall shear stress," in *Proc. 19th Int. Conf. Solid-State Sens., Actuators Microsyst. (TRANSDUCERS)*, Jun. 2017, pp. 938–941.
[10] B. Freidkes, D. A. Mills, C. Keane, L. S. Ukeiley, and M. Sheplak, "Development of a two-dimensional wall shear stress sensor for wind tunnel applications," in *Proc. AIAA Scitech Forum*, San Diego, CA, USA, Jan. 2019, p. 2045.
[11] D. Mills, "Microscale sensor structure with backside contacts and packaging of the same," U.S. Patent 10461239, Oct. 29, 2019.
[12] D. Mills, W. C. Patterson, B. Freidkes, C. Keane, and M. Sheplak, "Characterization of a fully-differential, dual-axis, capacitive wall shear stress sensor system for low-speed wind tunnels," in *Proc. AIAA Aviation*, Dallas, TX, USA, 2019, p. 2811.
[13] H. Weinberg, "Dual axis, low g, fully integrated accelerometers," *Analog Dialogue*, vol. 33, no. 1, pp. 1–2, 1999.
[14] M. Sheplak, A. Padmanabhan, M. Schmidt, and K. Breuer, "Dynamic calibration of a shear stress sensor using Stokes-layer excitation," *AIAA J.*, vol. 39, no. 5, pp. 819–823, May 2001.

Brett R. Freidkes was born in Huntington, New York, USA, in 1992. He received the B.S. and M.S. degrees in mechanical engineering from the University of Florida, Gainesville, where he is currently pursuing the Ph.D. degree in mechanical engineering. His research interests include the development of MEMS devices for aerodynamic applications.

David A. Mills was born in Evansville, IN, USA, in 1985. He received the B.S. degree in mechanical engineering from the University of Evansville in May 2008, and the M.S. degree in mechanical engineering and the Ph.D. degree in mechanical engineering from the University of Florida (UF) in December 2010 and December 2014, specializing in the area of high-temperature microelectromechanical systems (MEMS). From 2008 to 2014, he was a Research Assistant with the UF Interdisciplinary Microsystems Group. He concluded an appointment at UF as a Postdoctoral Research Associate in January 2016. He is currently the President of the Interdisciplinary Consulting Corporation (IC2), where he has been an employee since 2014. His current research focuses on microelectromechanical systems (MEMS) microphone, pressure sensor, and shear stress sensor development using capacitive, optical, and piezoelectric sensing technologies. He holds 1 patent, has published more than 25 conference articles and presentations, and is currently a member of the American Institute of Aeronautics and Astronautics (AIAA) Aerodynamic Measurement Technology Technical Committee.

William C. Patterson was born in Merritt Island, FL, USA, in 1989. He received the B.S., M.S., and Ph.D. degrees in electrical and computer engineering from the University of Florida, Gainesville.

From 2015 to 2017, he was a Senior Engineer with the Neutron Generator Division, Sandia National Laboratories. Since 2017, he has been a Senior Engineer with Interdisciplinary Consulting Corporation leading the electrical engineering team. He is an author on 11 publications and 2 inventions. His research interests include high-precision instrumentation in the fields of micro-magnetics, analog electronic test systems, and physical measurement MEMS sensors for aerospace applications.

Philip M. Fournier was born in Tallahassee, FL, USA, in 1985. He received the B.S. degree in chemistry from Florida State University and the M.S. degree in chemistry from the University of Pittsburgh, specializing in carbon nanomaterials. After working as a Process Engineer at the Thomas J. Watson Research Laboratory, IBM, Yorktown Heights, NY, he joined IC2 in 2018 as a MEMS Fabrication Process Engineer. His research interests include development of fabrication, packaging, and calibration processes for MEMS microphones and wall shear stress sensors.

Mark Sheplak (Member, IEEE) received the B.S., M.S., and Ph.D. degrees in mechanical engineering from Syracuse University, Syracuse, NY, USA, in 1989, 1992, and 1995, respectively. He is currently a Professor holding joint appointments at the Department of Mechanical and Aerospace Engineering and the Department of Electrical and Computer Engineering, University of Florida (UF). Prior to joining UF in 1998, he was a Post-Doctoral Associate at the Microsystems Technology Laboratories, Massachusetts Institute of Technology, Cambridge, MA, USA, from 1995 to 1998. His current research focuses on the design, fabrication, and characterization of high-performance, instrumentation-grade, MEMS-based sensors and actuators that enable the measurement, modeling, and control of various physical properties. He is a member of the Multi-Functional Integrated System Technology Center and the Florida Center for Advanced Aero-Propulsion. He is an Associate Fellow of AIAA and a fellow of the Acoustical Society of America.